Hydrodynamic planetary thermosphere model I: the response of the Earth's thermosphere to extreme solar EUV conditions and the significance of adiabatic cooling effect

Feng Tian[1], James F. Kasting[2], Hanli Liu[3], Raymond G. Roble[3]

1. NASA Postdoctoral Program Fellow at NASA Astrobiology Institute

2. Department of Geosciences, 443 Deike, Penn State University, 16802, USA

3. High Altitude Observatory, National Center for Atmospheric Research, Boulder, CO 80307, USA

Abstract:

It has been suggested that the exobase temperature of early terrestrial planetary atmosphere could have reached over10,000 K (Kulikov et al. 2006). Although such high exobase temperatures should have caused the major gases at the exobase to experience fast Jeans escape and the thermosphere should have experience hydrodynamic flow, hydrostatic equilibrium has been assumed to be valid in models. In this paper we developed a multi-component hydrodynamic thermosphere model to study the Earth's thermosphere under extreme solar EUV conditions self-consistently. The model is validated against the observations and models for present Earth's thermosphere. Simulations show that if forced in hydrostatic equilibrium and maintaining the current composition, the Earth's thermosphere could experience a fast transition from hydrostatic state to a "blow-off" state when exposed to certain critical solar EUV fluxes. When hydrodynamic flow and the adiabatic cooling effect are included, atmospheric blow-off is not reached and the Earth's exobase temperatures decrease with increasing solar EUV fluxes beyond the critical solar EUV fluxes. The fast variations of the bulk motion velocities under different exobase temperatures suggests that the adiabatic cooling effect could have kept the exobase temperature lower than ~1000 K if light gases such as atomic hydrogen were the dominant species in the Earth's thermosphere. We propose that the hydrodynamic flow and the associated adiabatic cooling should have existed in the thermospheres of early and/or close-in terrestrial-like planets regardless of their composition and that the cooling effect must be included in the energy consideration in order to estimate the thermospheric structure correctly.

1. Introduction

Atmospheric escape is one important process to determine the evolutionary paths of planetary atmospheres. During the early stage of planetary atmosphere evolution, due to the extremely large solar EUV radiation flux from the young star, thermal escape probably was probably the dominant escape mechanism for light gases such as hydrogen. Hydrodynamic escape, caused by fast escape of major gases in planetary atmospheres, occurs as a result of the combination of large energy input into the planet atmosphere and a relatively weak planetary gravity field. Through hydrodynamic escape, Venus may have lost oceans of water to space (Kasting and Pollack 1983, Chassefière 1996). Pluto may be experiencing ongoing hydrodynamic escape due to its low gravity (McNutt 1989, Hubbard et al. 1990, Krasnopolsky 1999, Tian and Toon 2005). Observations of at least one transiting extrasolar planet show an extensive hydrogen cloud surrounding the planet, which can be explained by hydrodynamic escape (Vidal-Madjar et al. 2003, Tian et al. 2005a). The close-in extrasolar planets, so called "hot Jupiters", are experiencing so intense stellar radiations that their atmospheres could be evaporated in relatively short time scales, although the results of theoretical models are different by many orders of magnitudes (Yelle 2004, Tian et al. 2005a, Lammer). Noble gas isotopes (Ne and Xe) in Earth's atmosphere appear to have been fractionated by this process (Pepin, 1991). In addition, recent modeling of 1D single-gas (H2) hydrodynamic escape from the atmosphere of the early Earth (Tian et al. 2005b) has shown that the escape of hydrogen from early Earth could have been energy-limited instead of diffusion-limited, which might allow hydrogen concentration in early Earth's atmosphere to be many times greater than previously recognized – an important indication of the atmospheric environment in which life originated and evolved. In general, researches on hydrodynamic escape from planetary atmospheres are critical to better understand the evolution of planetary atmospheres.

An extreme case of hydrodynamic escape is the atmospheric "blow off", a state in which the thermal energy of major gases at the exobase exceeds their gravitational energy and the whole planetary atmosphere escapes rapidly (Öpik 1963). For the Earth's thermosphere, if the thermospheric temperature reaches ~5000 K (approximately the blow-off temperature of atomic hydrogen) and the dominant gas remains atomic oxygen, the thermosphere is NOT in a blow-off state. However, it is important to realize that a blow-off temperature being reached at the exobase is NOT the necessary condition for hydrodynamic flow to start in a planetary atmosphere. A good example is the theoretical modeling of the "slow" hydrodynamic escape of N2 from Pluto (Krasnopolsky 1999, Tian and Toon 2005). Although the exobase temperature is as low as ~60K, which makes the thermal energy of N2 more than a factor of 5 smaller than their gravitational energy, hydrodynamic escape of N2 can be started and maintained due to Pluto's weak gravity field. The New Horizon spacecraft, which is on its way to Pluto, will be able to provide in-situ observations of the hydrodynamic escape from Pluto's atmosphere.

Despite the importance of hydrodynamic escape from planetary atmospheres, because of the inherent complexity of the problem, the status of the current theoretical modeling efforts of this process is not satisfactory. Besides the large discrepancies on the hydrogen escape rate from close-in extrasolar planets and the difficulty related to applying the hydrodynamic equations into the tenuous exospheres, most models investigating the hydrodynamic escape from early terrestrial planets (Kasting and Pollack 1983, Chassefière 1996, Tian et al. 2005b) treat the hydrodynamic equations adequately but depend on parameterization of heating efficiency due to the lack of detailed radiative transfer treatments.

On the other hand, although detailed chemistry and radiative transfer treatments are included in the Earth's thermospherie models (Roble et al. 1987, Roble 1995, Smithtro and Sojka 2005a, 2005b) so that heating efficiency can be computed self-consistently, hydrostatic equilibrium is a fundamental assumption of these models. Although the assumption of hydrostatic equilibrium for the Earth's current thermospheres is largely reasonable, to extrapolate it to the study of the long term evolution of planetary atmospheres is questionable.

It is suggested that the young Sun emitted stronger EUV radiations: approximately 3, 6, and 10 times that of today at ~3, 3.5, and 3.8 billion years ago (Ribas et al. 2005). For a young Sun only a few hundred million years after its formation, its EUV radiation level could have been 100 times that of today. Recently a hydrostatic equilibrium model (Kulikov et al. 2006) has been applied to the early terrestrial planet's thermospheres under a much wider range of solar radiation levels (1—100 times that of today). For early Earth with the same atmospheric composition as that of today, the model obtained a thermospheric temperature of 5,000 K when solar radiation was ~3 times that of today and more than 10,000 K when solar radiation was greater than 10 times that of today (Kulikov et al. 2006). Even when increasing the CO2 content to 1000 times that of today, the exobase temperature in their model can still reach 5,000 K when solar radiation was ~10 times that of today. The Kulikov et al. model applies a constant heating efficiency of ~50% throughout the thermosphere, solves the thermal balance and diffusive equilibrium equations by including detailed radiative transfer considerations for the vibrational kinetics of radiating molecules. However, the extremely high thermospheric temperatures obtained in Kulikov et al. (2006) means that the thermosphere cannot be considered hydrostatic because of the significant Jeans escape of atomic oxygen (the dominant gas in the upper thermosphere of the present Earth).

When major gases in the thermosphere flow, the bulk motion of the atmosphere is not negligible and a hydrodynamic description of the thermosphere is necessary. It has been pointed out that the adiabatic heating and cooling related to the bulk motion of the atmosphere are important in the energy budget of the thermospheres of Venus and the Earth (Bougher et al. 1999, Bougher et al. 2002). For early terrestrial planets, the extreme solar radiation conditions would have caused the whole thermosphere to expand and the adiabatic cooling related to the expansion cannot be ignored.

Although some of the hydrodynamic escape models (Krasnopolsky 1999, Yell 2004) included detailed radiative transfer treatments, the chemical schemes in these models are designed for the atmospheres of either giant planets or Pluto, which restricted the applications of these models to more general targets, such as the terrestrial-like planets. The motivation of this work is to develop a general thermosphere model which can be applied to various types of planetary atmospheres while taking potentially important hydrodynamic flow and the associated adiabatic cooling effect into consideration. In this paper we developed a 1D multi-component hydrodynamic thermospheric model to explore the response of the Earth's thermosphere under extreme solar EUV radiation conditions. The details of the model are described in section2. In section 3 the model is validated against the observations (NRL mass spectrometer incoherent scatter radar extended model NRLMSISE-00, Hedin 1991) and existing theoretical models (Roble et al. 1987, Roble 1995, Smithtro and Sokja 2005a, 2005b). The responses of the Earth's thermosphere to extreme solar EUV radiations and the significance of the adiabatic cooling effect are the focuses of section 4. Section 5 and 6 are the discussion and conclusions.

2. Model descriptions

The model treats the whole thermosphere as a single background fluid with varying mean molecular weight. Similar to the treatment in Kasting and Pollack (1983), the model iteratively solves the momentum and energy equations of the background gas in a moving atmosphere. In order to treat the energy deposition self-consistently and avoid using parameterization of heating efficiency, the model includes both neutral and ion species. Time-independent diffusion equations are solved for 14 long-lived species and chemical equilibrium is applied to 18 short-lived species. The species and the corresponding boundary conditions are listed in Table 1. Quasi-neutrality is assumed in the model. The model includes 154 chemical reactions, collected from thermospheric models of the present Earth (Roble 1995, Smithtro and Sojka 2005a), Venus/Mars (Nagy et al. 1983, Barth et al. 1992, Fox and Delgano 1979), and extrasolar planets (Yelle 2004). The list of reactions, reaction rates, energy released/absorbed, and the references are included in Table 2. The lower boundary of the model is at ~95 km and the top boundary is the exobase, selected at an altitude where the mean free path is comparable to the scaleheight of the background gas.

The 1D hydrodynamic thermospheric model solves the continuity, momentum, and energy equations in a moving atmosphere. We start from the 1D time-dependent non-viscous hydrodynamic equation set in Tian et al. 2005:

$$
\begin{cases}
\dfrac{\partial(\rho r^2)}{\partial t}+\dfrac{\partial(\rho u r^2)}{\partial r}=0, \\
\dfrac{\partial(\rho u r^2)}{\partial t}+\dfrac{\partial(\rho u^2 r^2+pr^2)}{\partial r}=-\rho GM+2pr, \\
\dfrac{\partial(Er^2)}{\partial t}+\dfrac{\partial[(E+p)ur^2]}{\partial r}=-\rho uGM+qr^2+\dfrac{\partial}{\partial r}(\kappa r^2\dfrac{\partial T}{\partial r}),
\end{cases}
\qquad (1)
$$

with $E=\rho(u^2/2+e)$, $e=\dfrac{p}{\rho(\gamma-1)}$, $p=\rho RT$

Here ρ =gas density, r=distance from the planet center, u=bolk motion velocity of background gas, p=pressure, G=universal gravitational constant, M=mass of the planet, E=total energy density (which is the sum of the kinetic energy density and the internal energy density of the gas flow), κ=thermal conductivity, T=temperature, γ=adiabatic constant, R=molar gas constant, q=volume heating rate.

Because we are interested in the steady state solution, the continuity and the momentum equations are rewritten into the following density and wind equation:

$$
\frac{1}{\rho}\frac{d\rho}{dr}=-\frac{1}{T}\frac{dT}{dr}+\frac{1}{m}\frac{dm}{dr}-\frac{g}{u_0^2}-\frac{u}{u_0^2}\frac{du}{dr} \qquad (2)
$$

$$
\frac{1}{u}\frac{du}{dr}(1-\frac{u^2}{u_0^2})=\frac{1}{T}\frac{dT}{dr}-\frac{1}{m}\frac{dm}{dr}+\frac{g}{u_0^2}-\frac{2}{r} \qquad (3)
$$

Here $u_0^2=kT/m$, $g=GM/r^2$, and m=mean molecular weight.

If the variations of the mean molecular weight with time and space are ignored, the time-dependent energy equation can be reduced to the following equation:

$$\frac{1}{\gamma}\frac{\partial T}{\partial t}=\frac{1}{\rho C_p}[\frac{1}{r^2}\frac{\partial}{\partial r}(\kappa r^2\frac{\partial T}{\partial r})+q]-u(\frac{\partial T}{\partial r}-\frac{1}{\rho C_p}\frac{\partial p}{\partial r}) \quad (4)$$

This equation is similar to the energy balance equation in Yelle (2004) and can be reduced to equation 3 in Kasting and Pollack (1983) in the steady state. The last term on the RHS is adiabatic cooling term. The contributions of O, O_2, N_2, CO_2, H_2, H, and N are included in the expression of thermal conductivity κ and heat capacity C_p. Solving equations 2, 3, and 4 provides the macroscopic properties (ρ, T, u) of the background gas. Both ρ and T are fixed at the lower boundary. At the top boundary the bulk motion velocity u is associated with the escape velocities of the dominant gases, which is atomic oxygen and atomic nitrogen. Atomic oxygen is the dominant gas in current Earth's upper thermosphere. Smithtro and Sojka (2005b) pointed out that the concentration of atomic nitrogen increases by a factor of 4 when increasing the solar EUV flux from that of solar maximum condition by a factor of 2. Our calculations confirms the findings of Smithtro and Sojka (2005b) and shows (in section 4) that atomic nitrogen indeed becomes a species competing with atomic oxygen for the dominancy at the exobase under extreme solar EUV conditions. In each iteration T, u, and ρ are solved subsequently and the time step size is adjusted according to the variation of T and ρ.

The concentrations of species in the thermosphere are important because they not only change the heating and cooling functions, but also change the mean molecular weight, which affect the mass density distribution. To obtain the concentrations of neutral long-lived species, we take the minor constituents approximation approach in Kasting and Pollack (1983). A caveat of the minor constituent approximation is that the mutual influences of the diffusion fluxes of major species on each other and on the minor gases are ignored and errors in the estimate of the diffusion fluxes can be introduced. However, as demonstrated in section 3, this approach is adequate for the calculations of large scale thermospheric structures. By combining the flux equation in the minor constituent approximation and the continuity equation for species i in a moving atmosphere described by equation 2-4:

$$\begin{aligned} u_i - u = &-D_i\left[\frac{1}{n_i}\frac{\partial n_i}{\partial r} - \frac{1}{n}\frac{\partial n}{\partial r} + (1 - m_i/m)\frac{1}{p}\frac{\partial p}{\partial r} + \frac{\alpha_i}{T}\frac{\partial T}{\partial r}\right] \\ &- K\left[\frac{1}{n_i}\frac{\partial n_i}{\partial r} - \frac{1}{n}\frac{\partial n}{\partial r}\right] \end{aligned} \tag{5}$$

$$\frac{\partial n_i}{\partial t} + \frac{1}{r^2}\frac{\partial}{\partial r}(r^2 n_i u_i) = P_i - L_i \cdot n_i \tag{6}$$

the following diffusion equation for species i can be derived:

:

$$\begin{aligned} \frac{\partial C_i}{\partial t} = \frac{m_i P_i}{\rho} - L_i \cdot C_i - \frac{1}{\rho r^2}\frac{\partial}{\partial r}\Big[&\rho r^2 (K + D_i)\frac{\partial C_i}{\partial r} \\ &+ \rho r^2 (K + D_i)\frac{1}{m}\frac{\partial m}{\partial r} C_i \\ &+ \rho r^2 (\widetilde{\mathrm{H}}_i - u) C_i\Big] \end{aligned} \tag{7}$$

Here C_i, n_i, m_i, P_i, L_i are the mass mixing ratio, number density, mass, chemical production, and chemical loss for species i respectively. D_i is the molecular diffusion coefficient of species i in the background gas and the hard sphere approximation is used. K is the eddy diffusion coefficient. $\widetilde{\mathrm{H}}_i = D_i[(1 - m_i/m)\frac{1}{p}\frac{\partial p}{\partial r} + \frac{\alpha_i}{T}\frac{\partial T}{\partial r}]$. p = pressure. α_i is the thermal diffusion factor and is set to be -0.25, -0.3, -0.4 for H, H2, He respectively (Hunte and Strobel 1974, Banks and Kockarts 1973) and zeroes for all other long-lived species.

In hydrostatic equilibrium, $\widetilde{\mathrm{H}}_i = D_i[1/H_i - 1/H_a + \frac{\alpha_i}{T}\frac{\partial T}{\partial r}]$, where Hi and Ha are the scaleheight of species i and the background gas respectively, and the diffusion equation can be reduced to eq. 25 in Kasting and Pollack 1983 in the steady state.

For long-lived ions, the ambipolar diffusion equation (Schunk and Nagy 2000) is solved. The ambipolar diffusion coefficients are calculated according to Schunk and Nagy (2000) and we include the contributions of 5 neutral species (O, N, H, N2, and O2) for the computation of the momentum transfer collision frequencies.

The solar radiation spectrum used in this model is from 0.5 nm to ~400 nm. The spectrum in the X-ray and EUV wavelength (<105 nm) are from EUVAC (Richards et al. 1994). The spectrum between 105 nm and 175 nm is from Woods and Rottman (2002). The spectrum for longer wavelengths is from Rottman et al. (1986). The parameterization method developed by Solomon and Qian (2005) is used to calculate ionization and dissociation rates in the thermosphere. More than one activity proxy, including the 10.7 cm solar radio flux (F10.7) and its 81-day centered average (<F10.7>), have been used in literature to describe the variability of the solar spectrum in different phases of a solar cycle. In this paper we use the solar activity proxy P = (F10.7+<F10.7>)/2, defined by Richards et al. (1994). Similar to Smithtro and Sojka (2005a) we use P=70 for solar minimum and P=230 for solar maximum. Fig. 1 shows the solar spectrum and its variability in a solar cycle.

The calculations of the neutral volume heating rate q include all the neutral heating and cooling mechanisms in the global mean model for Earth's thermosphere (Roble et al. 1987, Roble 1995) except for the following: heating by auroral electrons, heating by gravity wave, and eddy heat conduction. These terms are small in the current Earth's thermosphere and are characterized by parameterizations which may not be applicable when extrapolated to extreme solar EUV conditions. The electron and ion energy considerations are similar to those in the global mean model (Roble et al. 1987, Roble 1995). Because these energy treatments are described in details in Roble et al. (1987) and Roble (1995), they are not repeated here (or we can add a separate paragraph here). We only summarize the differences between this model and the global mean model in Roble et al. (1987) and Roble (1995).

For the heating rates and photolysis rates in the Schumann-Runge bands of O2, Schumann-Runge continuum of O2, and the Hartley bands of O3, we replaced the parameterization in the global mean model by explicit calculations of solar radiations absorption in order to facilitate the extrapolation of the model to planetary atmospheres with different composition than current Earth. Solar radiations absorption by H2O and CO2 in the Schumann-Runge bands and Schumann-Runge continuum are explicitly calculated and included in the heating and photolysis rates. Excitations of molecules/atoms by electron collision are updated according to Schunk and Nagy (2000).

Starting from an initial condition, the model first solves chemical equilibrium for short-lived species and then solves the diffusion equation for long-lived species using tridiagonal solver. Then the sum of the mass mixing ratios of long-lived species is renormalized and the mean molecular weight is recalculated. The model then solves the energy equation of electrons and the background gas by using fixed lower boundary condition and zero-gradient upper boundary condition. To solve the wind equation 3, the model applies a finite bulk motion velocity at the top boundary, which is assessed by multiplying the Jeans escape velocities of long-lived gases with the corresponding mass mixing ratios at the exobase. The density equation 2 is solved by fixing the lower boundary ρ. The sizes of time steps are adjusted according to the variation of both T and ρ in order to facilitate fast convergence when the model is approaching steady state. The number densities of long-lived species are computed at the end of each iteration.

3. Model validations

Detailed comparisons of thermospheric models with the observations have been discussed extensively in Roble et al. (1987), Roble (1995), and Smithtro and Sojka (2005a). Fig. 2—4 show the profiles of the current Earth's thermosphere under solar minimum and maximum conditions. Generally, the results of our model under solar minimum and solar maximum conditions are close to those in previous works.

Figure 2 shows the calculated neutral, ion, electron temperature profiles and number density distributions of 5 long-lived species (O,O2,N2,He,H) in the thermosphere. Also plotted in Fig. 2 are the corresponding profiles in the globally averaged profiles from the empirical NRLMSISE-00 model (Hedin 1991). The neutral temperature profiles in the model are slightly colder than those observed. At solar minimum the exobase temperature is 671 K compared to 735 K in MSIS-00. At solar maximum the exobase temperature is closer, 1220 K compared to 1242 K in MSIS-00. The greatest discrepancy occurs at around 200 km altitude, where the model temperature is ~100 K lower than that in MSIS-00. The ion and neutral temperature calculated in the model are similar to those in previous studies. At ~200 km altitude the electron temperature peak value is ~1400 K, closer to that in Roble et al. (1987). The electron temperature at ~400 km is closer to the neutral temperature than that in earlier models, probably a reflection of the stronger collisional coupling between neutrals, ions, and electrons in the model. The profiles of neutral species in Fig. 2 are similar to those in MSIS-00 but the fitness is not as good as those in previous works. The discrepancies may be partially caused by the minor constituent approximation we used in the diffusion equation because the fitness of the three major species (O,O2,N2) are better.

Fig. 3a and 3c show the calculated profiles of 3 long-lived species (N4S, NO, and CO2) and 3 short-lived species (O3, O1D, and N2D) at solar minimum and solar maximum. These species are closely related to the heating and/or cooling calculations in the model. All species have profiles similar to those in previous works. The dotted curves are the N(4S) density profiles from MSIS-00. The model calculated N(4S) density profile closer to that in MSIS-00 at solar maximum than at solar minimum. The densities of N(4S), N(2D), and O(1D) are greater at solar maximum than at solar minimum due to stronger photodissociation rates, which is similar to the results in previous works. Fig. 3b and 3d show the electron density and the profiles of 5 ion species (O+, NO+, O2+, N+, H+, N2+)

at solar minimum and solar maximum. Similar to those in previous works, O^+ is the dominant ion species at high altitudes and both O_2^+ and NO^+ dominate at low altitudes. The peak electron densities at solar minimum and maximum are ~3×10^5 and ~2×10^6 cm^{-3}.

The total heating and cooling profiles as well as the contributions from important individual mechanisms are plotted in Fig. 4. The general shapes of these heating/cooling profiles and the importance of each heating/cooling mechanism are similar to those in Roble et al. (1987) and Roble (1995). At solar minimum, the dominant heating mechanism above ~250 km is the collisional heating by ambient electrons (e-i), followed by the heating by exothermal chemical reactions (Qc), which includes neutral-neutral and neutral-ion reactions. Between 190 km and 250 km, chemical heating is dominant, followed by electron collision heating. Below 190 km, chemical heating is still dominant but Joul heating becomes the second most important heating mechanism, whose peak contribution reaches ~30% at 110 km altitude. Heating from the O_2 absorption in the Schumann-Runge continuum begins to be important below ~150 km and reaches peak ~20% at 120 km. The dominant cooling at high altitudes is the molecular thermal conduction, supplemented by less than 20% contribution from atomic oxygen fine structure cooling (63 μm) at ~300 km. The dominant cooling agent at low altitudes is CO_2 through 15 μm IR radiation, which contributes ~10% total cooling at ~130 km and more than 90% below 110 km. The greatest contribution of NO through 5.3 μm non-LTE radiation (~15%) to the total cooling occurs at ~145 km. At solar maximum the most apparent change in the heating/cooling profiles other than the increase of total heating/cooling is the increased cooling contribution of NO in the lower thermosphere, which reaches ~80% at ~140 km. Previous work (Roble et al. 1987) has found the same dominant role of NO cooling at similar altitude at solar maximum. In general, contributions from different heating/cooling mechanisms in this model at both solar minimum and solar maximum are close to those in previous works.

Smithtro and Sojka (2005b) discussed the response of the Earth's ionosphere and thermosphere under extreme solar cycle conditions (EUV energy flux between 0.5 and 14.5 mW/m2) using their GAIT (global average ionosphere and thermosphere) model. Fig. 5a shows the relationship between the P index and the solar EUV energy flux. The energy fluxes corresponding to solar minimum, mean, and maximum are marked by crosses. Fig. 5b and 5c show the variations of the exobase temperature and the total electron content (TEC) with solar EUV flux. We note that the exobase temperature computed in this model is a slightly better linear function of the solar EUV flux in the energy flux range 2 to 15 mW/m2 than that in GAIT. For stronger solar EUV fluxes, the exobase temperature begins to show non-linearity in a similar way as demonstrated in GAIT. Fig. 5d shows the peak density variations of 4 ion species (O+, N+, NO+, and O2+) and electrons with solar EUV flux, which are good indicators of the behavior of the ionosphere in the model. In GAIT, the peak density of O+ reaches a local maximum at solar EUV energy flux ~11 mW/m2 and decreases slightly for stronger solar EUV fluxes. Smithtro and Sojka (2005b) examined the plateau feature and suggested that competing factors in both the production and loss of O+ are responsible. Our model confirms the slower increase of the O+ peak density when solar EUV flux increases beyond ~10 mW/m2. The peak densities of O+ and N+ in our model are less than a factor of 2 greater than those in GAIT when solar EUV energy flux reaches 15 mW/m2. In general the responses of the thermosphere/ionosphere in our model are similar to that in GAIT (Smithtro and Sojka (2005b).

4. Thermosphere expansion under extreme solar EUV conditions and the adiabatic cooling effect

In the previous section the model is validated against the current Earth's thermosphere through comparison with observations and previous models. In this section we expose the model to much stronger solar EUV radiation levels.

Fig. 6 shows the temperature profiles of the thermosphere under different solar EUV fluxes. When the energy input into the thermosphere/ionosphere system increases, the exobase expands. The response of the temperature profile is more complicated. For solar EUV fluxes smaller than ~5 times that of today (5xEUV), the peak temperature in the thermosphere occurs at the exobase level. For solar EUV fluxes greater than 5xEUV, the peak temperature still increases with energy flux but the upper part of the thermosphere begins to cool down as a result of increasingly significant adiabatic cooling effect. The more the energy flux input into the thermosphere, the lower the exobase temperature. This behavior is typical in the studies of hydrodynamic escape from planetary atmospheres (Watson et al. 1981, Kasting and Pollack 1983, Chassefiere 1996, Yelle 2004, Tian et al. 2005a, 2005b).

The significance of the adiabatic cooling effect is better illustrated in Fig. 7, where three heating/cooling mechanisms are plotted as functions of altitude. The 4 panels in Fig. 7 correspond to the situations in 4 solar EUV flux levels: 1x, 4.9x, 5.3x, and 9.8x that of today. The solid curves are the net heating profiles from radiative transfer calculations, which include all radiative heating mechanisms and all the IR cooling mechanisms described in previous sections. The long dashed curves are the molecular thermal conduction and the short dashed curves are the adiabatic cooling. It is clear that when solar EUV flux is smaller than ~5 times that of today, all through the system the net heating from radiative transfer calculations are balanced by thermal conduction. Adiabatic cooling is negligible due to the small bulk motion velocities. In the 5.3xEUV case, the adiabatic cooling becomes effective near the exobase and the significance of thermal conduction cooling begins to decrease. When energy flux continues to increase, the adiabatic cooling effect becomes greater and the temperature begins to decrease with altitude in the upper part of the thermosphere. The effect of thermal conduction in the upper part of the thermosphere becomes heating (comparable to that from radiative transfer process) instead of cooling in the large solar EUV flux cases.

In Fig. 8 we plot the exobase temperature, peak temperature, exobase altitude, and exobase bulk motion velocity as a function of solar EUV fluxes (normalized by EUV flux in solar mean condition). The figures suggest that the responses of the Earth's thermosphere to extreme solar EUV conditions can be divided into two regimes separated by solar EUV flux ~5 times that of today. In regime I, the thermosphere behaves similar to that demonstrated by GAIT model and our model in previous section. The peak temperature occurs at the exobase. Both the temperature and altitude at the exobase level increase nonlinearly with solar EUV flux. Analysis of our simulation results shows that atomic oxygen maintains its status as the dominant species at the exobase in regime I, with increasingly stronger competition from atomic nitrogen. The trend of the rapidly increased atomic nitrogen, due to the increased photodissociation of N2 and accelerated production through ion-neutral chemical reactions, was also observed in the GAIT model, where the concentration of atomic nitrogen increases by a factor of 4 when increasing the solar EUV flux from that of solar maximum condition by a factor of 2 (Smithtro and Sojka 2005b). Our calculations confirms this finding and suggests that the number density of atomic nitrogen indeed becomes comparable to that of atomic oxygen at the exobase at solar EUV flux close to 5 times that of today.

The thermosphere's response to extreme EUV conditions enters regime II when the solar EUV flux increases beyond ~5 times that of today. In this regime, the peak temperature does not occur at the exobase any more and the exobase temperature decreases with increasing solar EUV flux. The altitude and the bulk motion velocity at the exobase level, as well as the peak temperature, increase with slopes much slower than those near the end of regime I. Atomic nitrogen becomes the dominant species at the exobase and ions (O+ dominant) becomes increasingly important and eventually dominates the exobase.

The behavior of the bulk motion velocity at the exobase level changes more dramatically at the transition from regime I to regime II (Fig. 7d). Simulations show that the bulk motion velocity at the exobase increases from <10 cm/s to >1e3 cm/s when changing the P index from 750 to 800. This dramatic increase of the bulk motion velocity at the exobase is controlled by the fast increase of exobase temperature from ~5000 K to nearly 8000 K. More discussion on this transition will follow in section 5.

As discussed in section 3, the dominant heating mechanism for the upper thermosphere during a normal solar cycle is the electron collision heating to the neutral gases. Analysis of the energy budget of the thermosphere under extreme solar EUV fluxes suggest that the electron collision heating maintains its status as the dominant heating mechanism in the upper thermosphere. Because the electron collision heating depends on the temperature difference between the electrons and the neutrals, a correct solution of the electron temperature is critical in calculating the electron collision heating accurately. In this model we solve the energy equation of the electrons by assuming that the electrons are static – adiabatic cooling effect is ignored for electrons. This will cause overestimation of the electron temperature and the contributions to neutral heating. To estimate how the adiabatic cooling for electrons could have influenced the response of the Earth's thermosphere under extreme solar EUV conditions, a series of simulations were done by fixing the electron temperature to neutral temperature, which sets the electron collision heating to zero. The simulation results are plotted in Fig. 8 as dotted curves. These sensitivity tests suggest that the thermosphere expansion could occur in a much more moderate style but the exobase would still begins to cool down when solar EUV flux is increased to ~10 times that of today.

To better understand the influence of the adiabatic cooling effect, we forced the thermosphere to be in the hydrostatic equilibrium by exerting a small bulk motion velocity at the exobase level. The dashed curves in Fig. 8a and 8b represent the variation of the exobase temperature and peak temperature with varying solar EUV fluxes. Our simulations show that the thermosphere's response remains the same when solar EUV flux is small – hydrostatic equilibrium assumption is sound when the energy input into the thermosphere is limited. But as the solar EUV flux approaches ~5 times that of today (~10 times that of today when using zero electron collision heating), the exobase begins to expand and warm up violently. When exobase altitude and temperature increase, the atmospheric "blow-off" state is reached quickly and eventually the exobase vanishes. This explosive expansion of the exobase is accompanied and caused by the extremely high exobase temperature, which is consistent with the acceleration trend of the exobase temperature growth under smaller energy inputs. These sensitivity test results suggest that the Earth's thermosphere could have experienced a fast transition from hydrostatic equilibrium to "blow-off" when exposed to certain critical solar EUV conditions and hydrostatic equilibrium does not apply in those cases.

5. Discussion

As described in last section, when P index increases from 750 to 800, the exobase temperature climbs from ~5000 K to ~8000 K (Fig. 8a) and the exobase moves from ~3500 km altitude to ~7700 km. At the same time the bulk motion velocity jumps from <10 cm/s to > 1e3 cm/s. This dramatic change in the bulk motion velocity at the exobase (which marks a transition from static thermosphere to hydrodynamic flow) is due to the exponential dependence of the Jeans escape velocity on the exobase temperature and exobase altitude. In Fig. 9 we plotted the variations of the Jeans escape velocities as a function of exobase temperatures. The two solid curves (for exobase at 1 Earth's radius and 2 Earth's radii respectively) are for a hypothetical gas with molecular weight 15, which is the same as the background gas (dominated by atomic O and N) at the exobase in our model in high solar EUV conditions. Because the exobase level moves outward when the solar EUV flux increases, the actual direction in which the Jeans velocity grows is marked by a symbolic arrow, whose sharp slope is the cause of the dramatic increase of the bulk motion velocity in Fig. 8a.

Fig. 8a and 8d suggest that for a thermosphere with current Earth's specifications the velocity range in which hydrodynamic flow begins to be important is between 100 and 1000 cm/s. The corresponding temperature range is between 7000 and 8000 K. It is interesting to note that if the Earth's thermosphere were dominated by light gases such as atomic hydrogen, exobase temperature less than 1000 K would be adequate to generate Jeans escape velocity of ~1000 cm/s. Thus if the early Earth's atmosphere were dominated by hydrogen as suggested by Tian et al. (2005b), the exobase and peak temperature in the thermosphere would have been lower than ~1000 K. This hypothesis is in agreement with the hydrodynamic models for early Earth and Venus (Watson et al. 1981, Kasting and Pollack 1983, Chassefiere 1996, Tian et al. 2005b). In a way, hydrodynamic flow of major gases from planetary atmospheres could act a role of thermostats, as proposed by Bougher et al (2002) for the heat budgets of current terrestrial thermospheres, which can protect the atmospheres from blow-off too quickly and too early. More simulations will be needed to better evaluate this thermostat effect and to determine how low the exobase temperature indeed was.

We note that our simulation results with forced hydrostatic equilibrium do not agree with the hydrostatic thermosphere models of Kulikov et al. (2006), in which an exobase can always be found in solar EUV flux range between 1xEUV and 100xEUV. The Kulikov et al. model solves the heat balance equation by including the vibrational kinetics of radiating molecules (CO2, NO, CO, O3, OH, etc.) as well as the 63μm O line. Kulikov et al. (2006) also included an eddy thermal conduction cooling function and a heating function due to dissipation of turbulent energy. Because the heating and cooling profiles were not provided in Kulikov et al. (2006), it is difficult to compare our results with theirs. The IR cooling agents in our model (15-μm CO2, 6.3-μm NO, and 63-μm O) have been generally accepted as the dominant radiative cooling agents in the thermospheres of the Earth, Mars, and Venus (Gordiets et al. 1982, Roble et al. 1987, Roble 1995, Bougher et al. 2002). Further work is needed to determine whether or not the IR radiation from the other minor radiatively active molecules can be the cause the discrepancy. Despite the difference in finding the exobase under extreme solar EUV fluxes, the fact that the exobase temperatures in Kulikov et al. (2006) are greater than 6000 K for solar EUV flux greater than 5 times that of today supports our conclusion that hydrodynamic flow (driving by fast Jeans escape of major gases at the exobase level) should start and adiabatic cooling effect should be significant when exposing the Earth's thermospheres to extreme EUV radiation levels.

Kulikov et al. (2006) did realize the possible cooling effect of fast Jeans escape of hydrogen on the energy budget of the thermosphere. Simulations in this paper show that even if the terrestrial planets were “dry”, hydrodynamic flow and the associated adiabatic cooling can still be significant. Because the composition of the atmosphere is the same as that of today, the relative importance of the adiabatic cooling and the CO2 cooling for a CO2-rich planetary atmosphere (the topic of a subsequent paper) is not discussed here. However it is reasonable to conclude that without including the adiabatic cooling effect, the thermospheric structures of terrestrial planets in their evolutionary history cannot be predicted accurately and the derived escape rates of atmospheric gases might be flawed.

In this paper we concentrate on the response of the Earth’s thermosphere to extreme solar EUV conditions without changing the composition of the atmosphere. However, as we go back in time, the composition of the Earth’s atmosphere almost certainly was different from that of today. Thus the details of (such as what the critical solar EUV flux was, what the exobase temperature was, etc.) how the Earth’s thermosphere actually evolved in time will require future work.

The chemical scheme in this model includes most chemical reactions appeared in thermospheric models of Earth, Venus, Mars, and extrasolar planets. The momentum, temperature, and diffusion equations in the model can handle both hydrostatic and hydrodynamic situations. Thus the model developed in this work provides a good framework upon which future researches can be done to study the long term evolution of planetary atmospheres under various solar radiation conditions. To apply the model to terrestrial-like extrasolar planets, including water planets, will be interesting and important future works.

6. Conclusions

In this paper we developed a multi-component hydrodynamic thermosphere model to study the Earth's thermosphere under extreme solar EUV conditions self-consistently. The model is validated against the observations (NRLMSISE-00) and models (Roble et al. 1987, Roble 1995, Smithtro and Sojka 2005a) for present Earth's thermosphere. The model also agrees with theoretical models developed for moderately strong solar EUV fluxes (Smithtro and Sojka 2005b). In this paper we concentrate on the response of the Earth's thermosphere (with its current composition) to extreme solar EUV conditions. The model shows that

1) the Earth's thermosphere could experience a fast transition from hydrostatic state to a "blow-off" state if hydrostatic equilibrium is forced in the model. The transition occurs at certain critical solar EUV fluxes, the value of which depends on the treatment of the electron collisional heating of the neutral gas. When hydrodynamic flow and the adiabatic cooling effect are included, atmospheric blow-off is not reached and the Earth's exobase temperatures decrease with increasing solar EUV fluxes beyond the critical solar EUV fluxes – hydrodynamic flow and the associated adiabatic cooling cannot be ignored when studying the early thermospheres of the Earth.

2) The fast variations of the bulk motion velocities under different exobase temperatures suggests that the adiabatic cooling effect could have kept the exobase temperature lower than ~1000 K if light gases such as atomic hydrogen were the dominant species in the Earth's thermosphere. We propose that the hydrodynamic flow and the associated adiabatic cooling should have been important in the thermospheres of early and/or close-in terrestrial-like planets regardless of their composition and that the adiabatic cooling effect (acting as a thermostat) must be included in the energy consideration in order to estimate the thermospheric structure correctly.

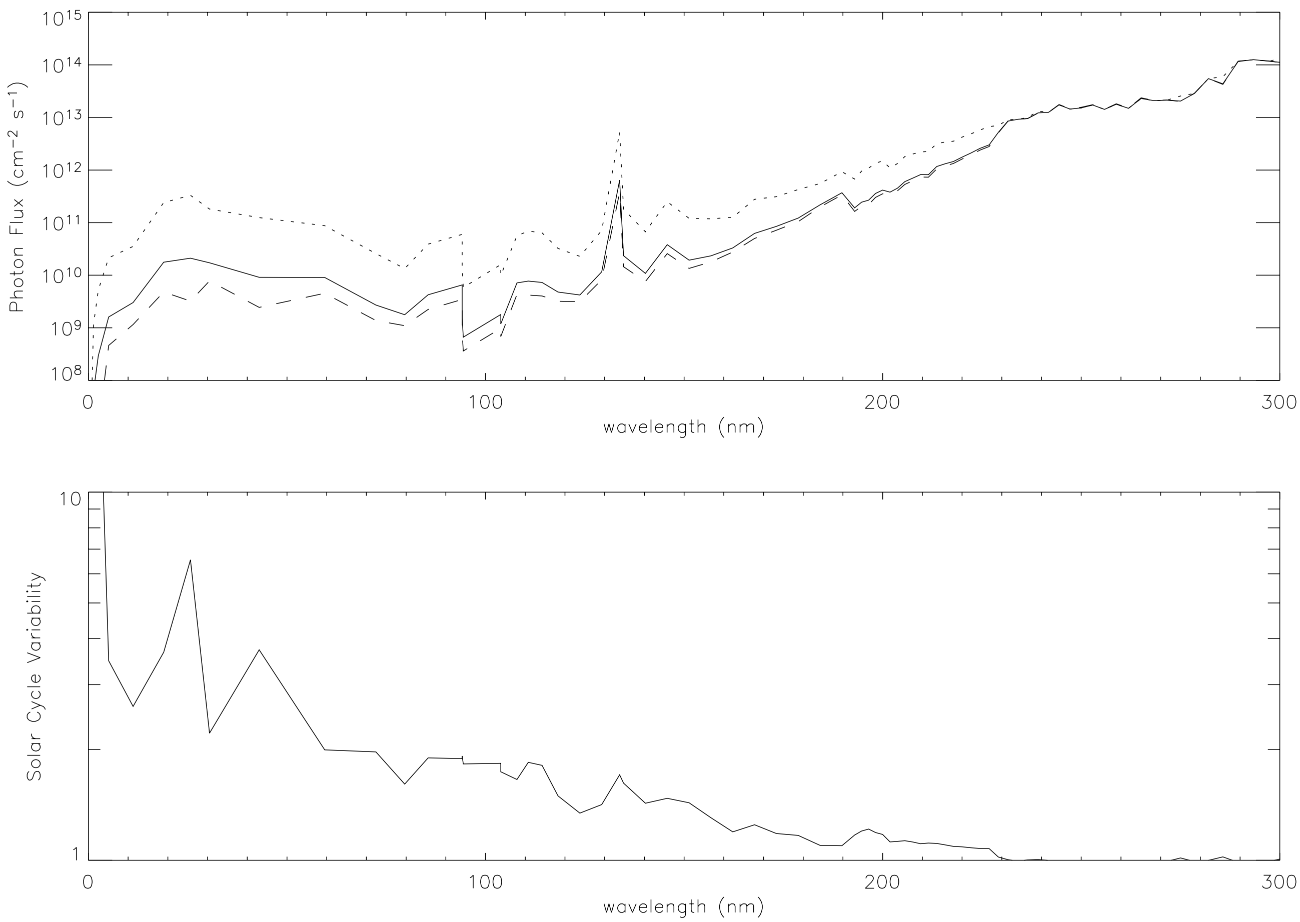

Fig. 1: solar spectrum between 0 and 300 nm and the variability in a solar cycle. Upper panel shows the photo fluxes in solar minimum (dashed), maximum (solid), and that in F107=3000 (dotted) conditions. Lower panel shows the ratio between solar maximum and minimum conditions.

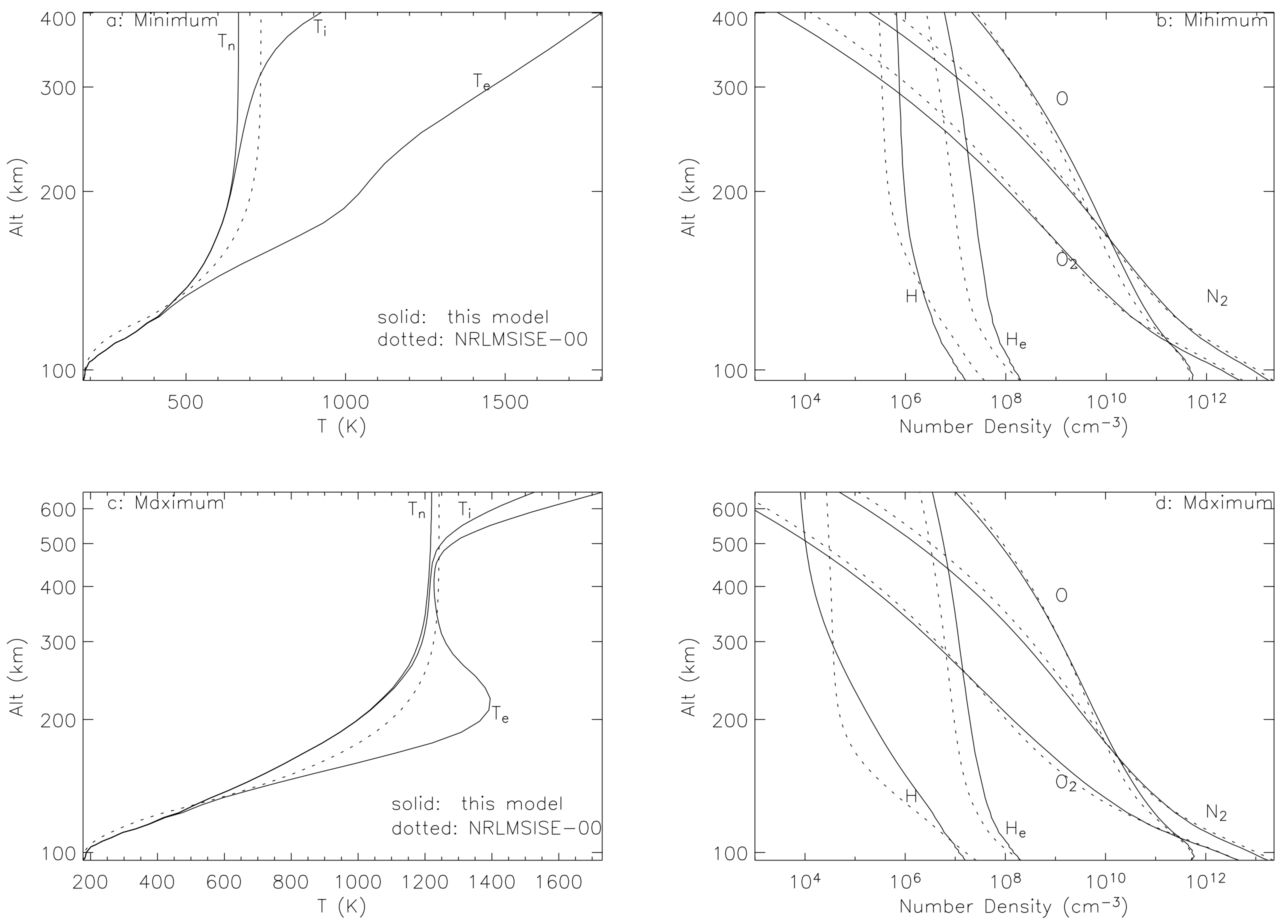

Fig. 2: temperature profiles and number density profiles of major neutral species in solar minimum and maximum conditions. Dotted curves are the globally averaged profiles from the empirical NRLMSISE-00 model.

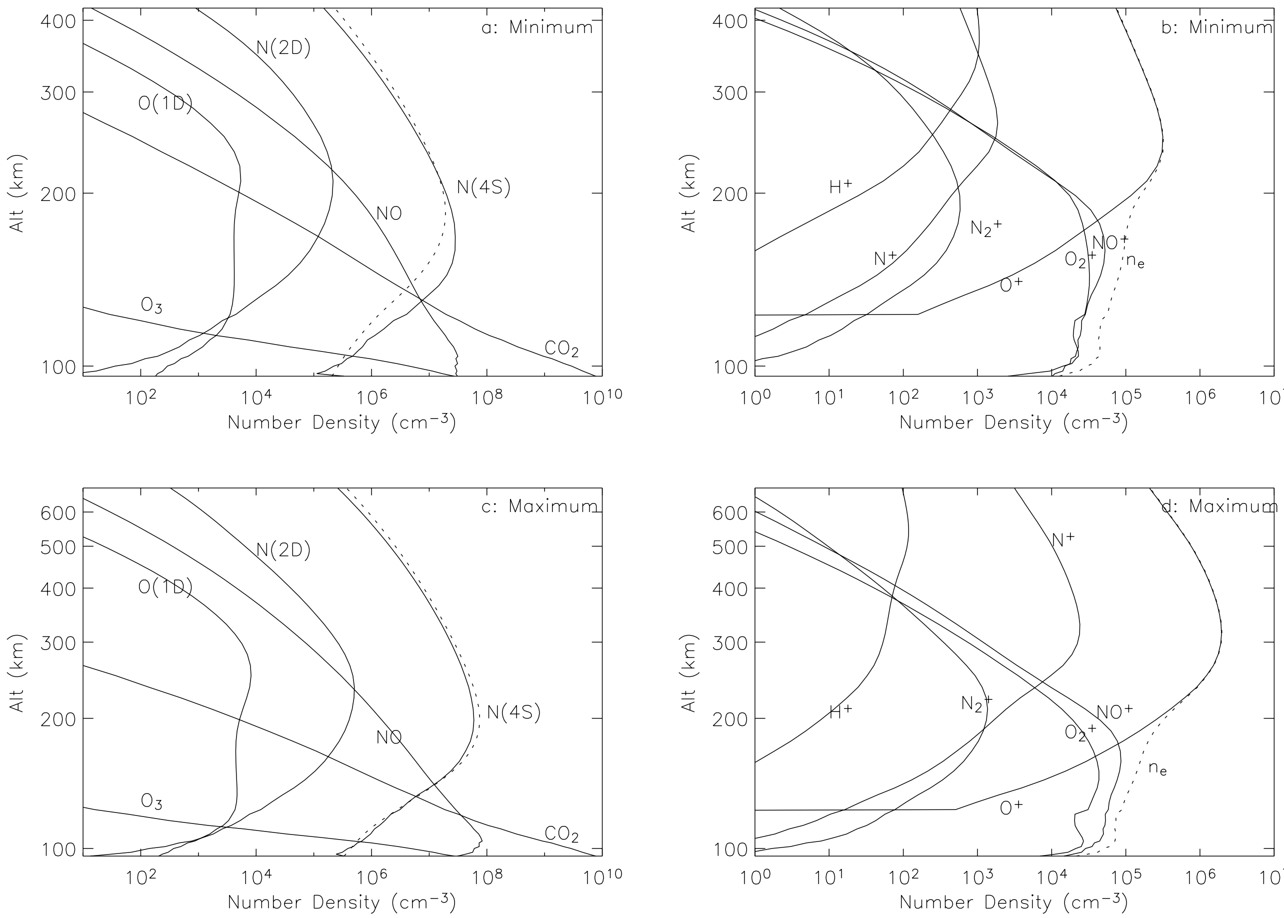

Fig. 3: number density profiles of N(4S), some minor neutral species, some major ion species, and electrons in solar minimum and maximum conditions. The dotted curves in 3a and 3c are the N(4S) distributions in NRLMSISE-00. The dotted curves in Fig. 3b and 3d are the electron densities.

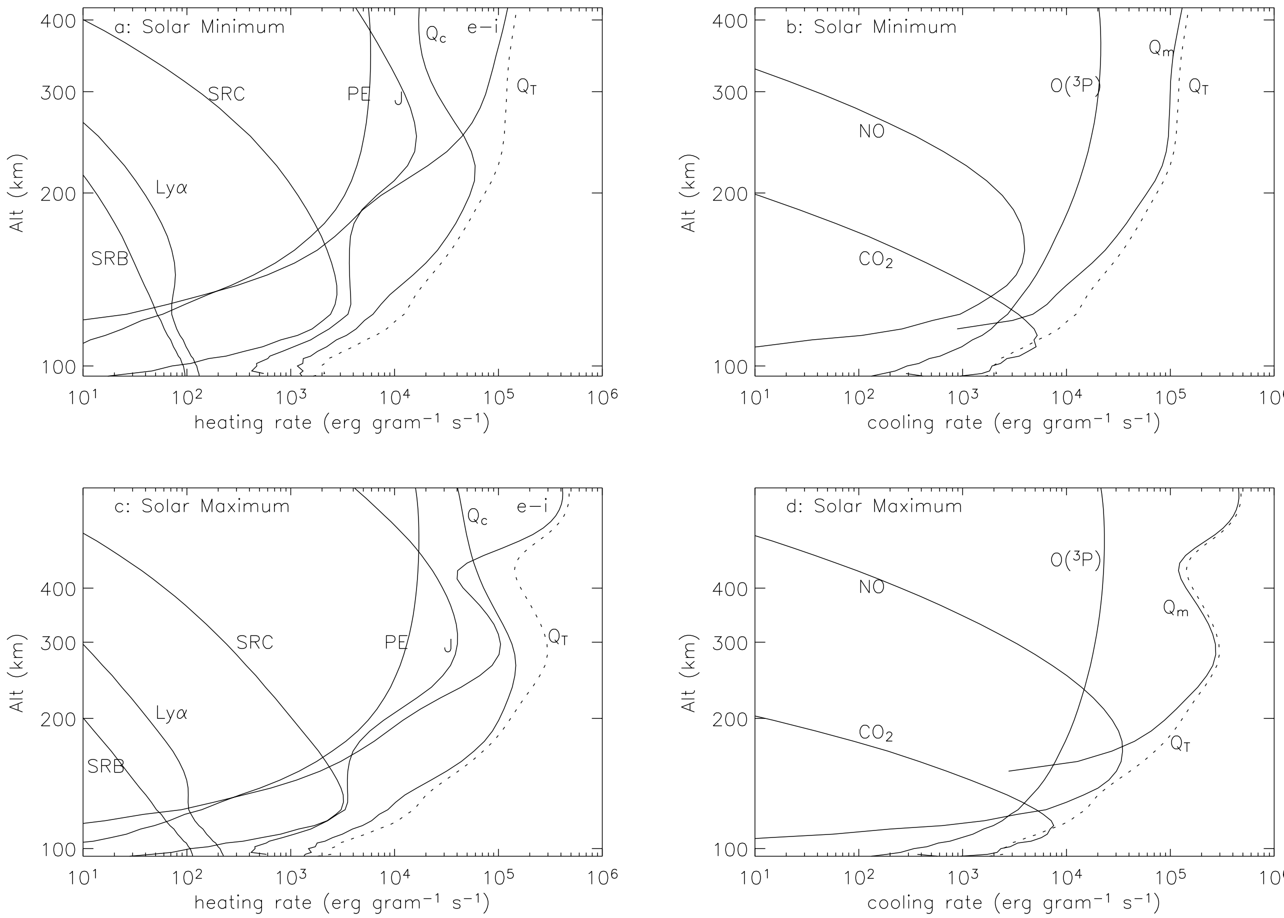

Fig. 4: heating and cooling rate profiles in solar minimum and solar maximum conditions. QT is the total heating rate, e-i is heating by collisions between thermal electrons, ions, and neutrals, Qc is the heating from ion-neutral and neutral-neutral chemical reactions, J is the Joul heating, PE is the direct heating from photoelectrons, SRC, SRB, and Lyα are heating from absorption in the Scumann-Runge continuum, Schumann-Runge bands, and Lyman α line respectively, Qm is the molecular thermal conduction cooling, O(3P) is the cooling from the fine structure of atomic oxygen, NO and CO2 are the radiative cooling from the 5.3-μm emission from NO and 15- μm emission from CO2 respectively.

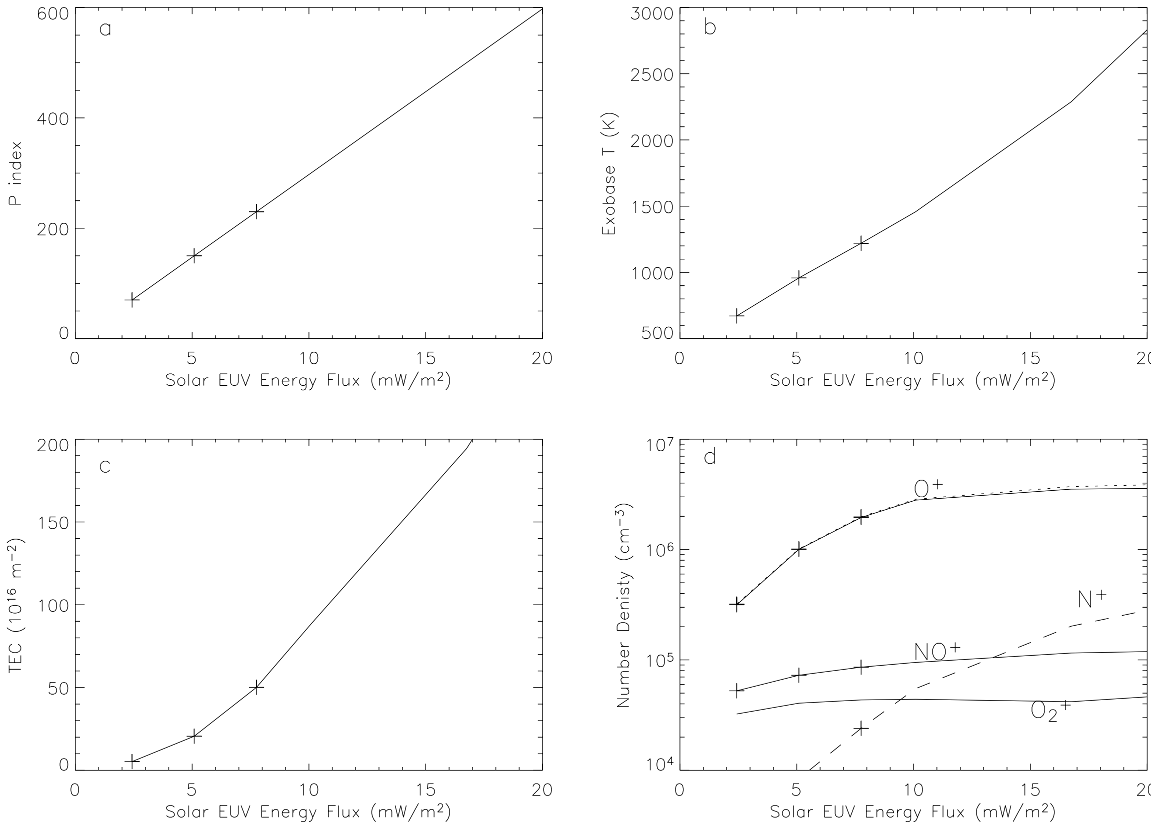

Fig. 5a: variations of solar EUV energy flux with P index. 5b: variation of exobase temperature with solar EUV flux. 5c: variation of TEC with solar EUV flux. 5d: variation of peak densities of major ion species with solar EUV flux, the dotted curve marks the variation of peak electron densities. In all panels the crosses correspond to the solar minimum, mean, and maximum values.

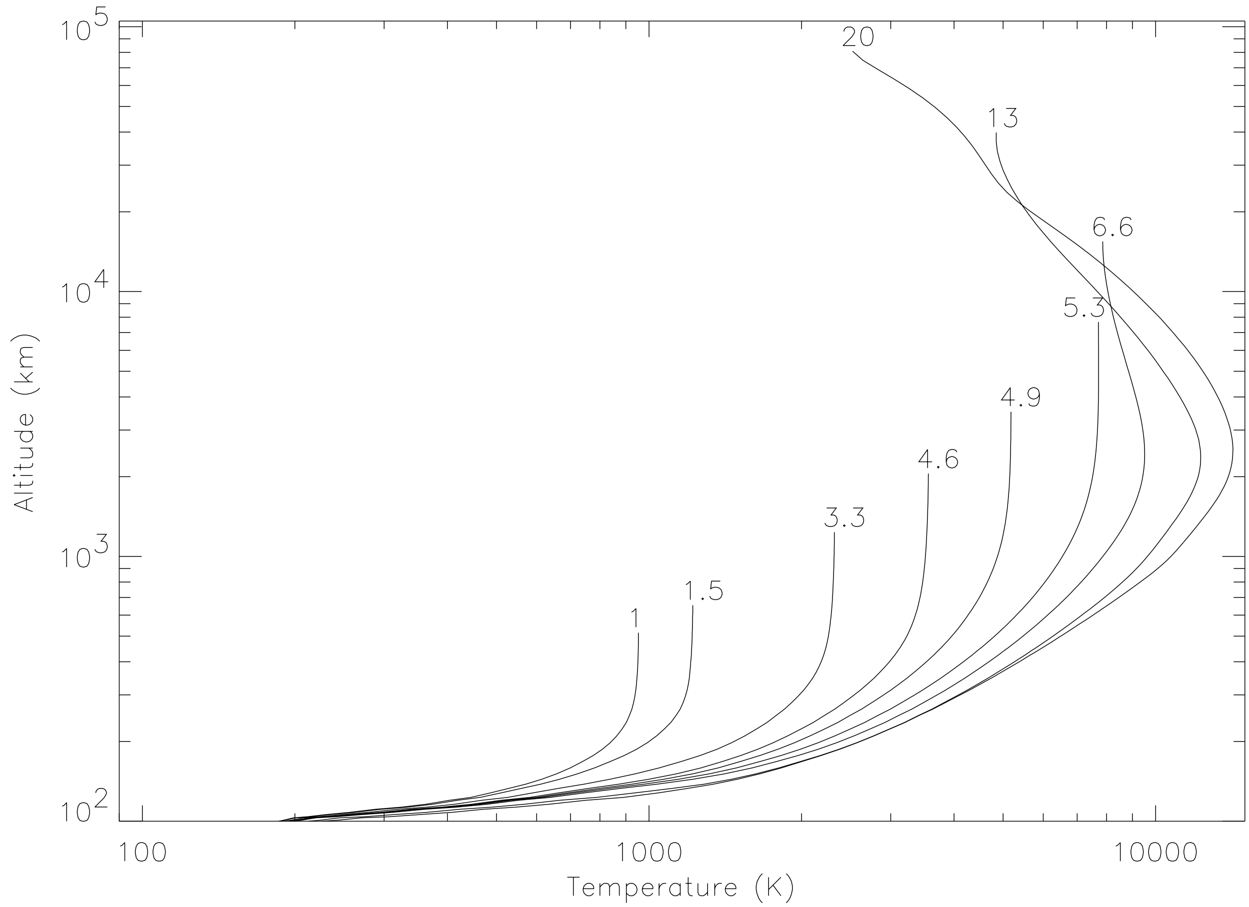

Fig. 6: temperature profiles in different solar EUV flux cases.

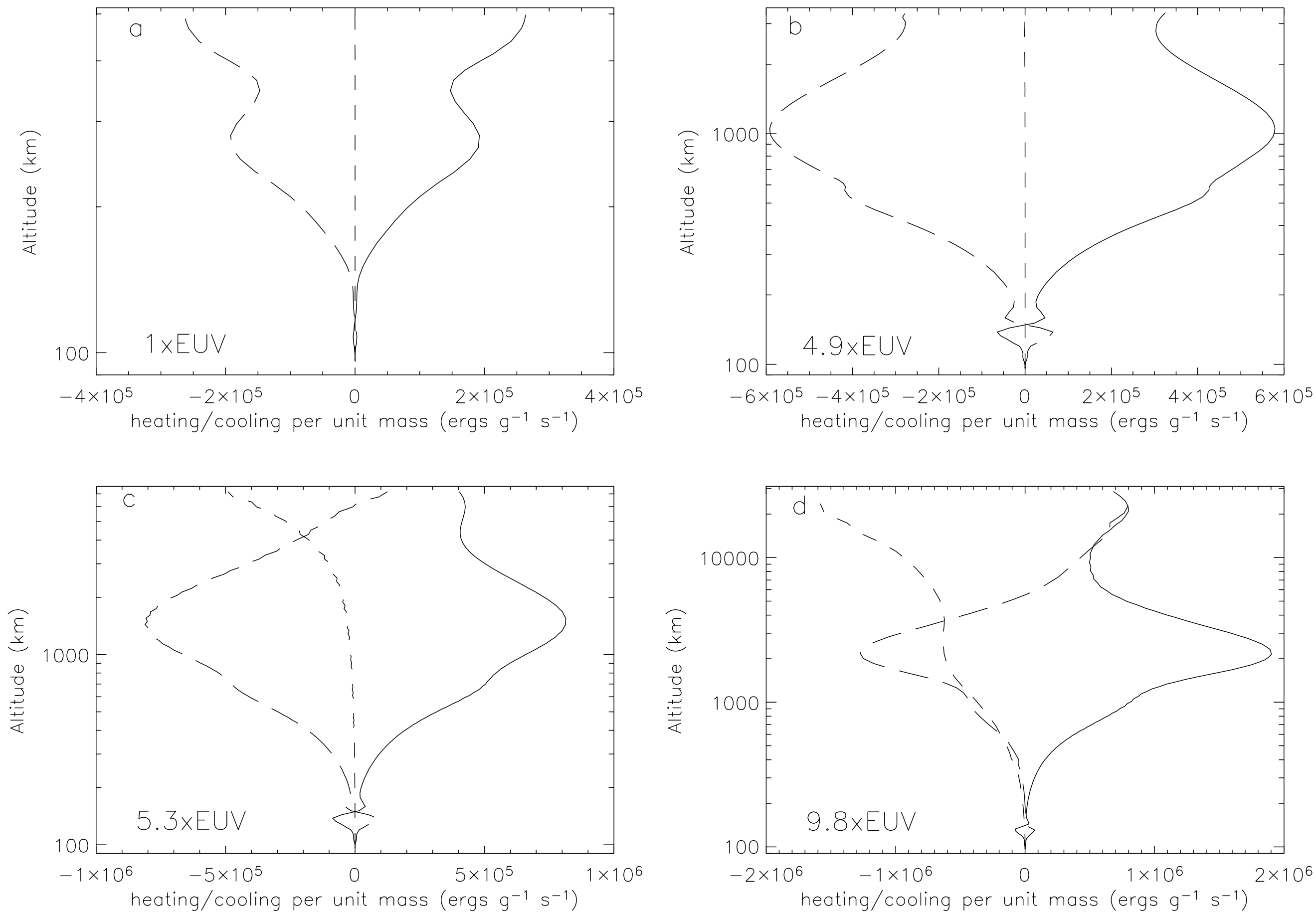

Fig. 7 profiles of heating and cooling mechanisms under different solar EUV flux cases (normalized by the solar EUV energy flux at solar mean). The solid curves are the net heating from radiative transfer calculations, including both the heating terms and IR cooling terms described in section 3. The long dashed curves are the molecular thermal conduction and the short dashed curves are the adiabatic cooling.

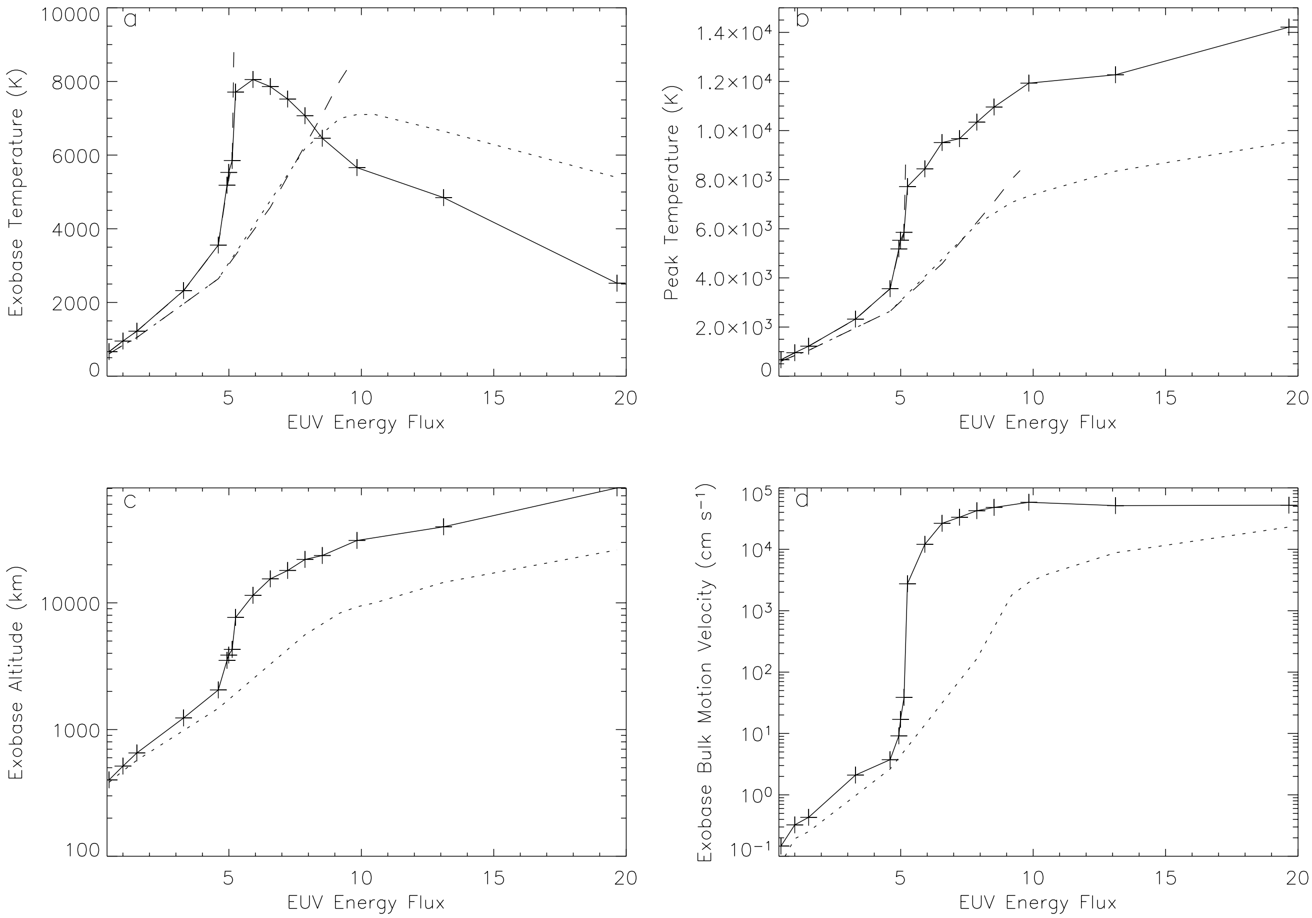

Fig. 8: variation of exobase temperature, altitude, bulk motion velocity, and the peak temperature with solar EUV flux. In all panels, the values on the horizontal axis are normalized by solar EUV flux at solar mean. The dotted curves in panel a, b, and c are obtained by fixing the electron temperature to the same as neutral temperature. The dashed curves are obtained by forcing hydrostatic equilibrium.

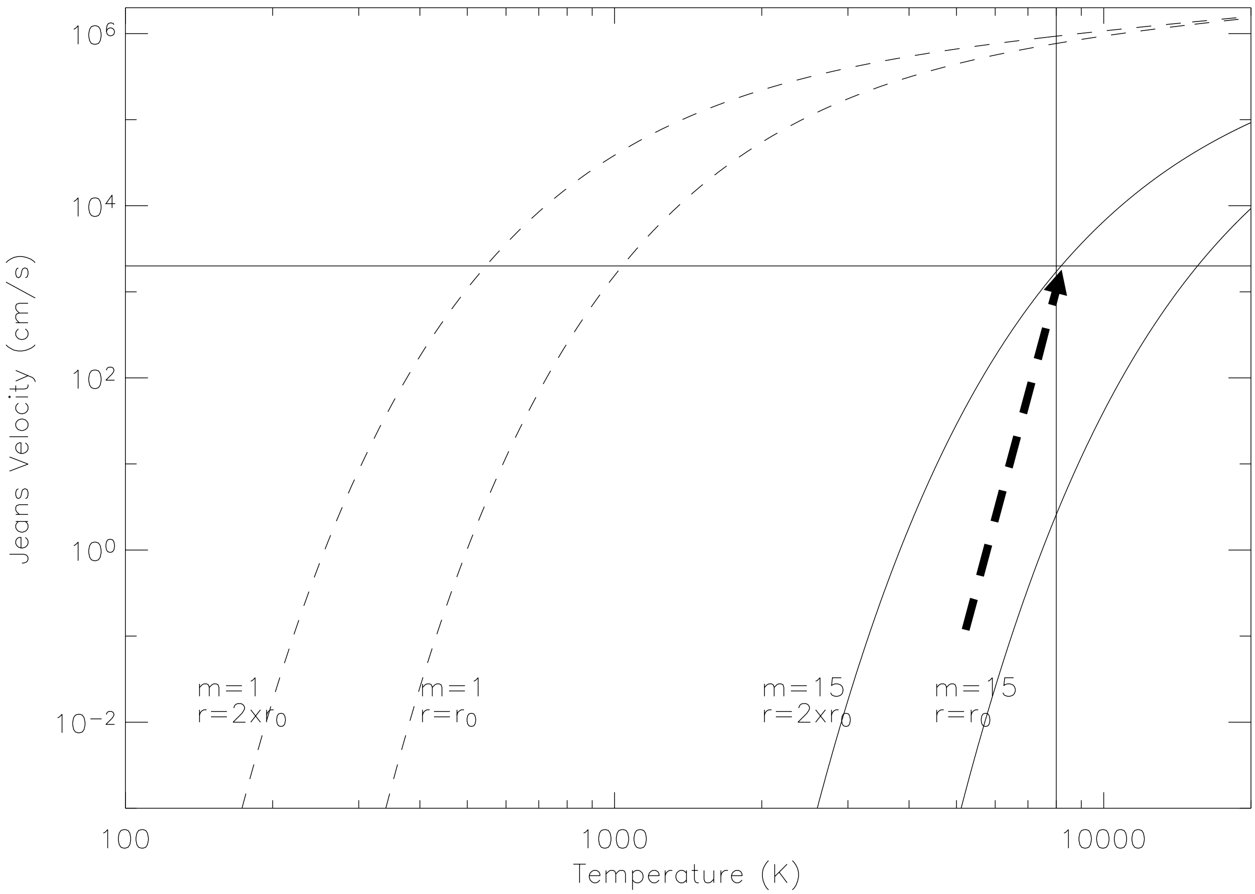

Fig. 9 Jeans escape velocity as a function of exobase temperature. The solid curves are for a hypothetical gas with molecular weight 15. The dashed curves are for atomic hydrogen. For each gas, two curves are plotted corresponding to different exobase altitude, one at the surface of the Earth, the other at 2 Earth radii.

Acknowledgement: We thank Drs. Y. Deng, J.H. Lei, L.Y. Qian, S. Solomon, and W.B. Wang for helpful discussions. F. Tian thanks the High Altitude Observatory of NCAR for providing the computing facilities. This work was partially supported by NASA Planetary Atmospheres Grant NNGO5GA53G.

References:

Banks, P.M. and G. Kocarts (1973), Aeronomy. Academic Press, New York and London.

Barth, C.A., A.I.F. Stewart, S.W. Bougher, D.M. Hunten, S.J. Bauer, and A.F. Nagy (1992), Aeronomy of the current Martian atmosphere. in Mars, Space Science Series, edited by H.H. Kieffer, B.M. Jakosky, C.W. Snyder, and M.S. Matthews, pp. 1054—1089, The University of Arizona Press

Bougher, S.W., S. Engel, R.G. Roble, B. Foster (1999), Comparative terrestrial planet thermospheres 2. Solar cycle variation of global structure and winds at equinox. JGR 104, 16591-16611

Bougher, S.W., R.G. Roble, T. Fuller-Rowell (2002), Simulations of the upper atmospheres of the terrestrial planets. In Atmospheres in the solar system: comparative aeronomy. Geophysical Monograph 130, edited by M. Mendillo, A. Nagy, J.H. Waite, pp 261-288, American Geophysical Union, Washington D.C.

Chassefiere, E. (1996), Hydrodynamic escape of hydrogen from a hot water-rich atmosphere: the case of Venus. JGR 101, 26039-26056

Fox, J.L. and A. Dalgarno (1979), Ionization, luminosity, and heating of the upper atmosphere of Mars. JGR 84, 7315-7333

Gordiets, B.F., Y.N. Kulikov, M.N. Markov, M.Y. Marov (1982), Numerical modeling of the thermospheric heat budget. JGR 87, 4504-4514

Kasting, J.F., and J.B. Pollack (1983), Loss of water from Venus. I. Hydrodynamic escape of hydrogen. Icarus 53, 479-508

Kulikov, Y.N., H. Lammer, H. Lichtenegger, T. Penz, D. Breuer, T. Spohn, R. Lundin, and H.K. Biernat (2006), A comparative study of the influence of the active young Sun on the early atmospheres of Earth, Venus, and Mars. Space Science Review, in press

Formichev, V.I., A.A. Kutepov, R.A. Akmaev, and G.M. Shved (1993), Parameterization of the 15 μm CO2 band cooling in the middle atmosphere (15-115 km). J. Atmos. Terr. Phys., 55, 7-18

Hedin, A.E. (1991), Extension of the MSIS Thermosphere Model into the Middle and Lower Atmosphere. JGR **96**, 1159

Hubbard, W.B., R.V. Yelle, J.I. Lunine (1990), Nonisothermal Pluto atmosphere models. Icarus 84, 1-11

Hunten, D.M. (1973), The escape of light gases from planetary atmospheres. Journal of the Atmospheric Sciences 30, 1481-1494

Hunten, D.M. and D.F. Strobel (1974), Production and escape of terrestrial hydrogen. Journal of the Atmospheric Sciences 31, 305-317

Kumar, S., D.M. Hunten, and J.B. Pollack (1983), Nonthermal escape of hydrogen and deuterium from Venus and implications for loss of water. Icarus 55, 369-389

McNutt, R.L. (1989), Models of Pluto's upper atmosphere. GRL 16, 1225-1228

Nagy, A.F., T.E. Cravens, and T.I. Gombosi (1983), Basic theory and model calculations of the Venus ionosphere, in Venus, Space Science Series, edited by D.M. Hunten, L. Colin, T.M. Donahue, and V.I. Moroz, pp.841—872, The University of Arizona Press

Roble, R.G., E.C. Rodley, R.E. Dickinson (1987), On the global mean structure of the thermosphere. JGR 92, 8745-8758

Roble, R. G. (1995), Energetics of the mesosphere and thermosphere, in The Upper Mesosphere and Lower Thermosphere: A Review of Experiment and Theory, Geophys. Monogr. Ser., vol. 87, edited by R. M. Johnson and T. L. Killeen, pp. 1 –21, AGU, Washington, D. C.

Schunk, R. W., and A. F. Nagy (2000), Ionospheres: Physics, Plasma Physics, and Chemistry, Cambridge Univ. Press, New York.

Smithtro, C.G., and J.J. Sojka (2005a), A new global average model of the coupled thermosphere and ionosphere. JGR 110, A08305, doi:10.1029/2004JA010781

Smithtro, C.G., and J.J. Sojka (2005b), Behavior of the ionosphere and thermosphere subject to extreme solar cycle conditions. JGR 110, A08306, doi:10.1029/2004JA010782

Tian, F., O.B. Toon, A.A. Pavlov, H. DeSterck (2005a), Transonoic hydrodynamic escape of hydrogen from extrasolar planetary atmospheres. ApJ 621, 1049-1060

Tian, F., O.B. Toon, A.A. Pavlov, H. DeSterck (2005b), A hydrogen-rich early Earth atmosphere. Science 308, 1014-1017

Tian, F., O.B. Toon (2005), Hydrodynamic escape of nitrogen from Pluto. GRL 32, L18201, doi:10.1029/2005GL023510

Watson, A.J., T.M. Donahue, and J.C.G. Walker (1981), The dynamics of a rapidly escaping atmosphere: applications to the evolution of Earth and Venus. Icarus 48, 150-166

Yelle, R.V. (2004), Aeronomy of extrasolar giant planets at small orbital distances. Icarus 170, 167-179

Yung, Y.L. and W.B. DeMore (1999), Photochemistry of planetary atmospheres. Oxford University Press, Oxoford